SLAC-PUB-7230
July 1996

Preliminary Measurements of the Time Dependence of $B^0_d - \overline{B^0_d}$ Mixing with Kaon and Charge Dipole Tags**

The SLD Collaboration*
Stanford Linear Accelerator Center
Stanford University, Stanford, CA 94309

Abstract

We report two preliminary measurements of the time dependence of $B^0_d - \overline{B^0_d}$ mixing using novel techniques with a sample of 150,000 hadronic Z^0 decays collected by the SLD experiment at the SLC. B decay vertices are reconstructed inclusively with a topological technique and the B hadron flavor at production is determined by exploiting the large left-right forward-backward asymmetry of $Z^0 \to b\,\overline{b}$ decays in combination with a jet charge technique. Two methods are used to tag the B flavor at decay. The first uses the charge of kaons attached to the B decay vertex and identified with the Cherenkov Ring Imaging Detector. The second measurement is based on the construction of a charge dipole of the topological vertices to separate the $B^0_d/\overline{B^0_d}$ decays by exploiting the $B \to D$ cascade charge structure. The measurement of the oscillation frequency yields $\Delta m_d = 0.58 \pm 0.07(\text{stat}) \pm 0.08(\text{syst})\ \text{ps}^{-1}$ and $0.56 \pm 0.08(\text{stat}) \pm 0.04(\text{syst})\ \text{ps}^{-1}$ for the kaon and dipole tags respectively.

Contributed to the XXVIII International Conference on High Energy Physics, Warsaw, Poland, July 25-31, 1996

**This work was supported by Department of Energy contracts: DE-FG02-91ER40676 (BU), DE-FG03-92ER40701 (CIT), DE-FG03-91ER40618 (UCSB), DE-FG03-92ER40689 (UCSC), DE-FG03-93ER40788 (CSU), DE-FG02-91ER40672 (Colorado), DE-FG02-91ER40677 (Illinois), DE-AC03-76SF00098 (LBL), DE-FG02-92ER40715 (Massachusetts), DE-AC02-76ER03069 (MIT), DE-FG06-85ER40224 (Oregon), DE-AC03-76SF00515 (SLAC), DE-FG05-91ER40627 (Tennessee), DE-AC02-76ER00881 (Wisconsin), DE-FG02-92ER40704 (Yale); National Science Foundation grants: PHY-91-13428 (UCSC), PHY-89-21320 (Columbia), PHY-92-04239 (Cincinnati), PHY-88-17930 (Rutgers), PHY-88-19316 (Vanderbilt), PHY-92-03212 (Washington); the UK Science and Engineering Research Council (Brunel and RAL); the Istituto Nazionale di Fisica Nucleare of Italy (Bologna, Ferrara, Frascati, Pisa, Padova, Perugia); and the Japan-US Cooperative Research Project on High Energy Physics (Nagoya, Tohoku).

1 Introduction

$B_d^0 - \overline{B_d^0}$ mixing occurs via a second order weak interaction in complete analogy to the mixing observed in the $K^0 - \overline{K^0}$ system. The flavour eigenstates of the B^0 are written in terms of the mass eigenstates B_1 and B_2, as $B^0 = (B_1 + B_2)/\sqrt{2}$ and $\overline{B^0} = (B_1 - B_2)/\sqrt{2}$. Unlike the neutral kaon system the difference between the B meson lifetimes is expected to be small. Hence, the probability that a meson created as a B^0 ($\overline{B^0}$) will decay as a B^0 ($\overline{B^0}$) after proper time t can be written as

$$P_u(t) = \frac{\Gamma}{2} e^{-\Gamma t} \left(1 + \cos \Delta m_d \, t\right) , \tag{1}$$

where Δm_d is the mass difference between the mass eigenstates, Γ is the decay width for both states and P_u denotes the probability to remain 'unmixed'. The effects of CP violation are assumed to be small and are neglected. Similarly, the probability that the same initial state will 'mix' and decay as its antiparticle is

$$P_m(t) = \frac{\Gamma}{2} e^{-\Gamma t} \left(1 - \cos \Delta m_d \, t\right) . \tag{2}$$

In this paper, we present two measurements of the $B_d^0 - \overline{B_d^0}$ mixing parameter Δm_d based on a sample of 150,000 hadronic Z^0 decays collected by the SLD experiment between 1993 and 1995 at the SLC (SLAC Linear Collider). Both measurements exploit the large longitudinal polarization of the electron beam. Average polarizations for the 1993 and 1994/95 running periods are $(63.0 \pm 1.1)\%$ and $(77.2 \pm 0.5)\%$ respectively.

Most components of the SLD detector were used in this analysis. The Liquid Argon Calorimeter (LAC) was used for triggering and event shape measurement. It provides excellent solid-angle coverage ($|\cos\theta| < 0.84$ and $0.82 < |\cos\theta| < 0.98$ in the barrel and endcap regions, respectively). The LAC is divided longitudinally into electromagnetic and hadronic sections. The energy resolution for electromagnetic showers is measured to be $\sigma/E = 15\%/\sqrt{E(GeV)}$, whereas that for hadronic showers is estimated to be $60\%/\sqrt{E(GeV)}$. Tracking is provided by the Central Drift Chamber (CDC) and the CCD pixel Vertex Detector (VXD) with maximal track reconstruction efficiency for $|\cos\theta| < 0.74$. Charged tracks are first reconstructed in the CDC and linked with clusters in the VXD, and then a combined fit is performed. The momentum resolution of the combined fit is $\sigma_{p_\perp}/p_\perp = \sqrt{(0.01)^2 + (0.0026/p_\perp)^2}$, where $p_\perp$ is the track momentum transverse to the beam direction in GeV/c. The impact parameter resolution was measured using the miss distance between the two tracks in $Z^0 \to \mu^+\mu^-$ decays. This yields a high-momentum single-track resolution of 11 μm in the plane perpendicular to the beam direction (xy plane) and 38 μm in the plane containing the beam axis (rz plane). One of the analyses presented here, utilizes the particle identification capabilities of the Cherenkov Ring Imaging Detector (CRID). The CRID contains both liquid and gas radiators to provide efficient $\pi/K/p$ separation over a wide momentum range.

The position of the micron-sized SLC Interaction Point (IP) in the xy plane is reconstructed with a measured precision of $\sigma_{IP} = (7 \pm 2)$ μm using tracks in sets of ~ 30 sequential hadronic Z^0 decays. The z position of the Z^0 primary vertex is determined on an event-by-event basis using the median z position of tracks at their point-of-closest-approach to the IP in the xy plane. The simulation described below estimates a precision of ~ 52 μm in this quantity for $Z^0 \to b\,\bar{b}$ decays [1].

The time-dependent mixing measurements rely on a Monte Carlo simulation based on the JETSET 7.4 event generator [2] and the GEANT 3.21 detector simulation package [3]. The b-quark fragmentation followed the Peterson *et al.* parametrization [4]. B mesons were generated with mean lifetime $\tau = 1.55$ ps and B baryons with $\tau = 1.10$ ps. B hadron decays were modelled according to the CLEO B decay model [5] tuned to reproduce the spectra and multiplicities of leptons, charmed hadrons, pions, kaons, and protons, measured at the $\Upsilon(4S)$ by ARGUS and CLEO [6, 7]. B baryon and charmed hadron decays were modelled using JETSET with, in the latter case, branching fractions tuned to existing measurements [8]. Monte Carlo samples used in this paper consist of approximately 500,000 $Z^0 \to b\,\bar{b}$ and 100,000 $Z^0 \to udsc$ events.

Hadronic Z^0 event selection requires at least 7 CDC tracks which pass within 5 cm of the IP in z at the point of closest approach to the beam and which have $p_\perp > 0.2$ GeV/c. The total energy of the tracks passing these cuts must be greater than 18 GeV. These requirements on the CDC tracking information remove background from $Z^0 \to l^+l^-$ events and two-photon interactions. In addition, the thrust axis determined from clusters in the calorimeter must pass $|\cos\theta| < 0.71$, within the acceptance of the vertex detector, and at least three tracks must have two or more linked VXD hits. These selection requirements yield a data sample of 96,000 hadronic Z^0 decays.

Well measured tracks are selected in these events. The CDC tracks must begin at a radius $r < 39$ cm, and have $\geq$40 hits to insure that the lever arm provided by the CDC is appreciable. The CDC tracks are also required to extrapolate to within 1 cm of the IP in xy, and within 1.5 cm in z to eliminate tracks from interaction with the detector material. The fit of the track must satisfy (χ^2/d.o.f.< 5). At least one good VXD link is required, and the combined CDC/VXD fit must also satisfy (χ^2/d.o.f.< 5). The track must have $p_\perp > 0.4$ GeV/c.

2 Topological Vertex Reconstruction

The excellent 3D vertexing capabilities of SLD are exploited to identify B hadron vertices produced in hadronic Z^0 decays with high efficiency. A novel topological vertexing technique for reconstructing the secondary vertices produced by weakly decaying hadrons in charged particle jets is employed [9]. The topological vertex

reconstruction is applied separately in each event hemisphere using tracks selected as described above (the event thrust axis determined by calorimetry clusters is used to divide the event into two hemispheres). The vertices are reconstructed in 3D co-ordinate space by defining a vertex probability $V(\mathbf{r})$ at each position $\mathbf{r}$. The helix parameters for each track i are used to describe the 3D track trajectory as a Gaussian tube $f_i(\mathbf{r})$, where the 2D width of the tube is the uncertainty in the measured track location close to the IP. $V(\mathbf{r})$ is defined as a function of the $f_i(\mathbf{r})$ such that it is sensitive to the track multiplicity at $\mathbf{r}$ and is small in regions where less than two tracks (required for a vertex) have significant $f_i(\mathbf{r})$. A further function $f_0(\mathbf{r})$ is used to describe the location and uncertainty of the IP. This function is combined with the $f_i(\mathbf{r})$ in the definition of $V(\mathbf{r})$ in order to later identify the tracks forming the primary vertex. Maxima are found in $V(\mathbf{r})$ and clustered into spatial regions using a resolution criterion such that two maxima are resolved if the value of $V(\mathbf{r})$ on a straight line between the maxima falls below 60% of the value of $V(\mathbf{r})$ at either maxima. Tracks are associated with these resolved regions to form a set of topological vertices.

The inclusive efficiency for reconstructing at least one secondary vertex in a b hemisphere is $\sim$ 50% (cf. an efficiency of $\sim$ 15% in charm hemispheres and $\sim$ 3% in light quark hemispheres), while the efficiency for finding both a secondary and a tertiary vertex is $\sim$ 5%. The vertex reconstruction efficiency in b hemispheres rises from 0% near the IP to 80% at 3 mm from the IP beyond which it remains constant. For the b hemispheres containing secondary vertices, a 'seed' vertex is chosen to be the non-primary topological vertex furthest from the IP. The seed vertex is rejected if it consists of two oppositely charged tracks with an invariant mass in the range 491–505 MeV/c^2 to remove $K^0_s \to \pi^+\pi^-$ decays. If such a rejected seed was a topological tertiary vertex then the two tracks are discarded and the secondary vertex is used as the seed vertex.

A vertex axis is formed by a straight line joining the IP to the seed vertex (see Fig. 1). The transverse impact parameter of a track to the vertex axis, T, and the distance from the IP along the vertex axis to this point, L, are calculated for all tracks [9]. Monte Carlo studies show that tracks which are not associated with the seed vertex but which pass T$<$ 0.1 cm and L/D$>$ 0.3 are more likely to be associated with the B decay sequence than to have an alternative origin. Hence such tracks are added to the set of tracks in the seed vertex to form the reconstructed B vertex. This secondary vertex contains tracks from both the B and cascade D decays. The distance from the IP to the vertex fit to all of the tracks now forming the secondary vertex is the reconstructed decay length.

The mass M of the reconstructed vertex is calculated by assuming each track forming the secondary vertex has the mass of a pion. The transverse component of the total track momentum in the vertex relative to the vertex axis (P_T) is calculated in order to determine the P_T added mass:

$$\mathrm{M}_{P_T} = \sqrt{M^2 + P_T^2} + |P_T|. \qquad (3)$$

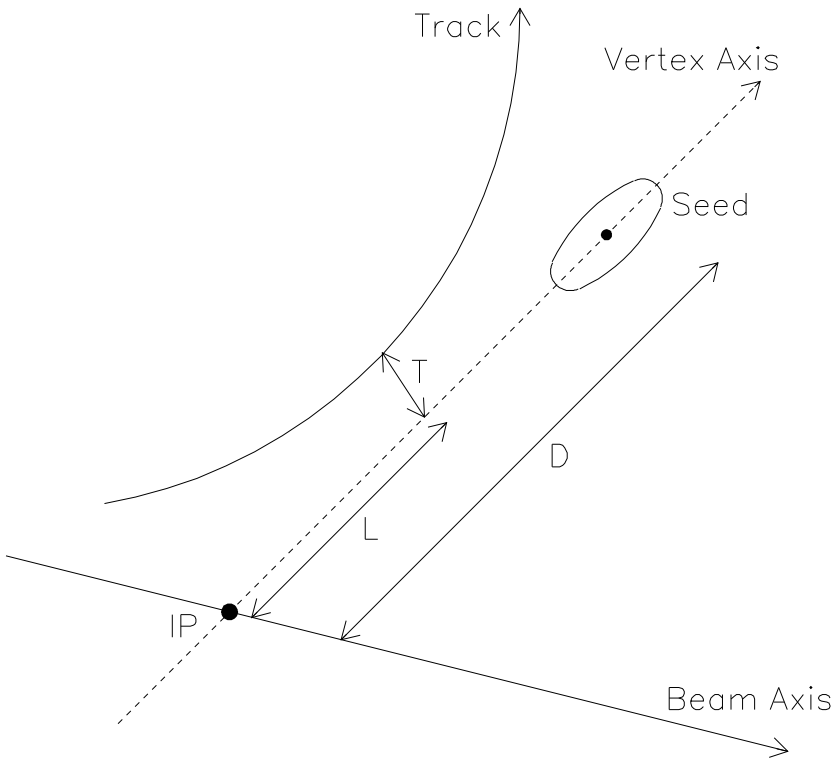

Figure 1: Impact parameter of a track with respect to the vertex axis.

This quantity is the minimum mass the decaying hadron could have in order to produce a vertex with the quantities M and P_T. The direction of the vertex axis is varied within the 1.5 σ limits constraining the axis at the measured IP and reconstructed seed vertex such that the P_T is minimized within this variation. This procedure prevents non-B background vertices acquiring a high M_{P_T} due to a fluctuation in the measured P_T. The accurate 3D vertexing and precisely measured IP at SLD allow significant gain in the b-tag efficiency with high purity using this technique.

A comparison of the reconstructed vertex M_{P_T} between data and Monte Carlo is shown in Fig. 2 for vertices with decay length greater than 1 mm. This figure shows that a large fraction of the charm and light flavour contamination in the sample is eliminated by requiring $\mathrm{M}_{P_T} > 2$ GeV/c^2. This mass cut yields a sample of 16803 decays with $Z^0 \to b\,\overline{b}$ purity of 93% and efficiency of 36% (including the vertex reconstruction efficiency) and is applied for the remainder of this paper. For decay lengths greater than 1 mm, the purity increases to 97% with an efficiency of 33%. However, no decay length cut is applied in the mixing analysis.

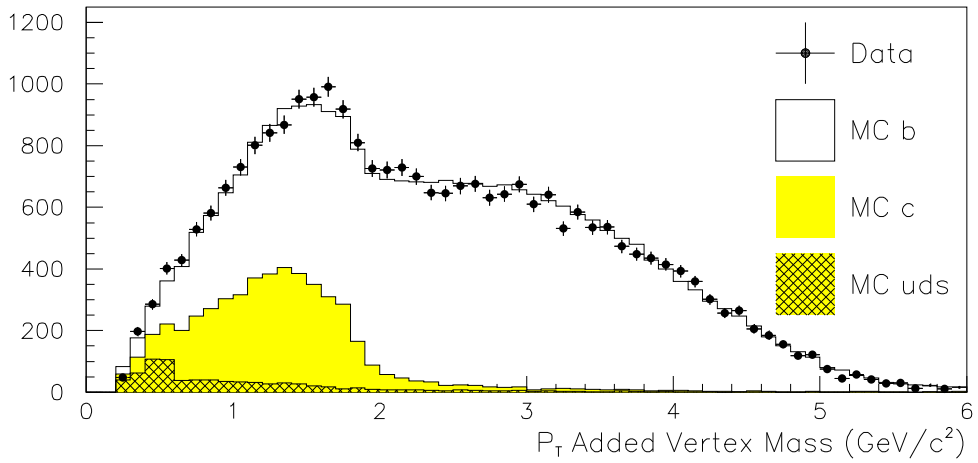

Figure 2: M_{P_T} of reconstructed vertex for data (points) and Monte Carlo (histograms).

3 Flavor Tagging

In order to measure the time dependence of $B_d^0 - \overline{B_d^0}$ mixing, it is necessary to determine the B_d^0 or $\overline{B_d^0}$ flavor at both production (t=0) and decay. The initial state flavor tagging takes advantage of the large polarized forward-backward asymmetry for $Z \rightarrow b\,\bar{b}$ decays in addition to a jet charge technique. The final state flavor tagging uses either the charge of identified kaon tracks attached to the secondary vertex or the charge dipole which is defined in terms of all the vertex tracks.

3.1 Initial State Tagging

The large forward-backward asymmetry for $Z^0 \rightarrow b\bar{b}$ decays is used as a nearly 100% efficient tag of the initial state flavor. The polarized forward-backward asymmetry $\tilde{A}_{FB}$ can be described by

$$\tilde{A}_{FB} = 2A_b \, \frac{A_e + P_e}{1 + A_e P_e} \, \frac{\cos\theta_T}{1 + \cos^2\theta_T} \; , \tag{4}$$

where $A_b = 0.94$ and $A_e = 0.155$ (Standard Model values), P_e is the electron beam longitudinal polarization, and θ_T is the angle between the thrust axis and the positron beam direction (the thrust axis is signed such that it points in the same hemisphere as the reconstructed vertex). Thus, left- (right-)polarized electrons tag b ($\bar{b}$) quarks in the negative hemisphere, and $\bar{b}$ (b) quarks in the positive hemisphere (see Fig. 3a). This yields an average correct tag probability of 76% (62%) for an average electron polarization $P_e = 77\%$ (63%). The probability for correctly tagging a b quark at production is expressed as

$$P_A(b) = \frac{1 + \tilde{A}_{FB}}{2} \; . \tag{5}$$

A jet charge technique is used in addition to the polarized forward-backward asymmetry. For this tag, tracks in the hemisphere opposite that of the reconstructed vertex are selected. These tracks are required to have momentum transverse to the beam axis $p_\perp > 0.15$ GeV/c, total momentum $p < 50$ GeV/c, impact parameter in the plane perpendicular to the beam axis $\delta < 2$ cm, distance between the primary vertex and the track at the point of closest approach along the beam axis $\Delta z < 10$ cm, and $|\cos\theta| < 0.8$. With these tracks, an opposite hemisphere momentum-weighted track charge is defined as

$$Q_{opp} = \sum_i q_i \left|\vec{p}_i \cdot \hat{T}\right|^\kappa \ , \tag{6}$$

where q_i is the electric charge of track i, $\vec{p}_i$ its momentum vector, $\hat{T}$ is the thrust axis direction, and κ is a coefficient chosen to be 0.5 to maximize the separation between b and $\overline{b}$ quarks. A clear separation can be observed as shown in Fig. 3b. The probability for correctly tagging a b quark in the initial state of the vertex hemisphere can be parametrized as

$$P_Q(b) = \frac{1}{1 + e^{\alpha Q_{opp}}} \ , \tag{7}$$

where the coefficient $\alpha = -0.27$, as determined using the Monte Carlo simulation. This technique yields an average correct tag probability of 67% and is independent of the polarized forward-backward asymmetry tag.

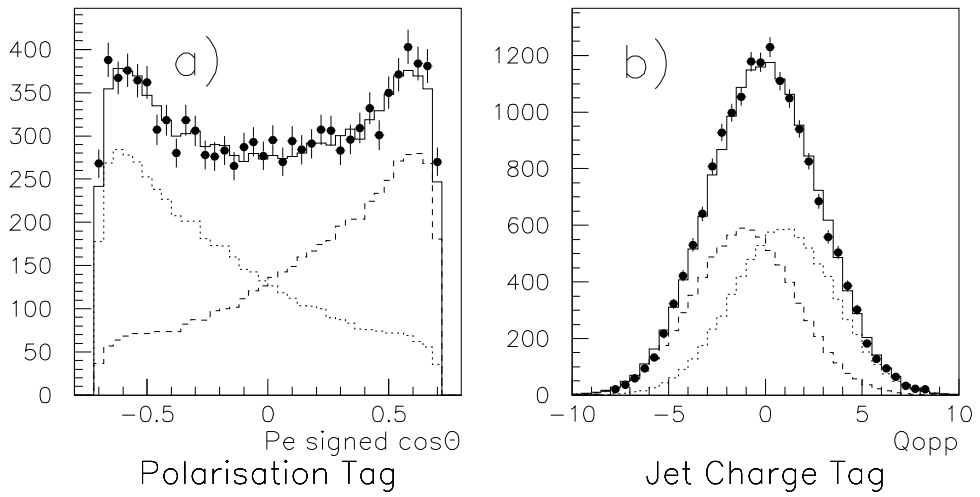

Figure 3: Initial state tag variables, polarization-signed $\cos\theta$ of the thrust axis and opposite hemisphere jet charge, for data (points) and MC (solid line) with MC b and $\overline{b}$ quark components (dashed and dotted lines respectively).

Fig. 3 shows the performance of the initial state $b/\overline{b}$ quark separation for both tags after topological vertex selection. The two initial state tags can be combined to form an overall initial state tag. The correct sign probability for the combined tag can be written as the normalized product of the independent tags:

$$P_i(b) = \frac{P_A(b)P_Q(b)}{P_A(b)P_Q(b) + [1 - P_A(b)][1 - P_Q(b)]} \ , \tag{8}$$

which yields an overall average correct tag probability of 84%.

3.2 Final State Kaon Tag

The final state flavor tagging relies on the characteristics of B meson decays. The first technique uses the charge of identified kaons attached to the secondary vertex and exploits the fact that most B decays occur via the dominant quark transition $b \to c \to s$. Therefore, the electric charge of kaons produced in B decays can be used to determine the charge of the b quark at decay. The correlation between kaon charge and B flavor is diluted by decays of the type $B \to DDX$ and by $s\bar{s}$ production in D decays. However, the rate of right-sign kaon production is large and has been measured to be $(82 \pm 5)\%$ in B_d^0 decays [10].

Kaon identification is performed with the CRID using information from both liquid and gas radiators. Only tracks attached to the secondary vertex are considered for kaon identification. The CRID is required to be operational in the region surrounding the tracks. Additional cuts are applied to guarantee acceptably low misidentification rates while keeping the efficiency high. Tracks are required to have $p > 0.8$ GeV/c and $|\cos\theta| < 0.68$. For each track above pion threshold in the gas radiator ($p > 2.5$ GeV/c), we require either that the extrapolated track matches with a minimum-ionizing signal in the CRID or that a ring was detected in the liquid radiator (4 or more hits) for that particular track. The latter set of requirements is designed to remove tracks which undergo large scattering before exiting the CRID. These cuts keep 65% of all secondary vertex tracks. Separation between pion, kaon and proton hypotheses is carried out on the basis of differences in logarithms of likelihood ($\mathcal{L}_i$ with $i = \pi, K, p$) between these hypotheses. The quantity $\mathcal{L}_i$ depends on the measured Cherenkov angles for hits in the CRID that are associated with the track as well as on the number of such hits. The kaon identification requires $\mathcal{L}_K - \mathcal{L}_\pi > 3$ to select kaons and $\mathcal{L}_K - \mathcal{L}_p > -5$ to reject well-identified protons. These differences correspond to demanding a minimum 2.4 σ separation between K and π hypotheses and 3.2 σ separation between p and K hypotheses. The log likelihoods used in this analysis are combined log likelihoods from both liquid and gas radiators. This combination enhances the identification performance in the momentum range 2.5 to 4.0 GeV/c where the kaon spectrum from B decays peaks (this range corresponds to the overlap region between the two radiators).

The particle identification performance has been studied and calibrated with a pure sample of pion tracks from $K_s^0 \to \pi^+\pi^-$ decays. This study determines an additional $\sim 5\%$ in the $\pi \to$"K" misidentification in the data, an increase for which the Monte Carlo simulation is corrected.

The final state tag uses the sum of identified kaon charges in the vertex, $\sum Q_K$. The requirement $\sum Q_K < 0$ (> 0) tags $\overline{B_d^0}$ (B_d^0) decays. Vertices for which $\sum Q_K = 0$, representing 12% of vertices with at least one identified kaon, are thus rejected. This

K^-/K^+ tag is available for some 1/3 of the selected secondary vertices with a correct final tag probability of $P_K(b) = 77\%$ (81%) for $\overline{B^0_d}$ (B^-_u) decays, as determined using our simulation. The number of decays passing the above selection criteria and used for the kaon tag measurement is 5694.

3.3 Final State Charge Dipole Tag

The $B \to D$ cascade charge structure is exploited to separate the final state $B^0/\overline{B}^0$ decay flavor. An enhanced sample of B^0_d decays is first selected by requiring that the total charge of the tracks associated with the vertex is equal to zero. In addition, there must be no lower quality tracks (tracks failing the good track selection but with $p_\perp > 0.2$ GeV/c and impact parameter resolution $\sqrt{\sigma^2_{xy} + \sigma^2_z} < 700\mu$m) passing the criterion to be attached to the seed vertex.

The direction of the vertex axis (Fig. 1) is adjusted in order to minimize the summed impact parameters ($\sum_i \mathrm{T}_i$) of the tracks in the secondary vertex. It is required that the mean of the track impact parameters T_i is less than 50μm at this minimum. The charge dipole δq of the vertex is defined as the relative displacement between the weighted mean location of the positive tracks and of the negative tracks along the vertex axis taking each track at its point of closest approach to the vertex axis (see Fig. 1):

$$\delta q = \frac{\sum_i^+ w_i L_i}{\sum_i^+ w_i} - \frac{\sum_i^- w_i L_i}{\sum_i^- w_i} \tag{9}$$

where the first (second) term sums over all positive (negative) tracks in the vertex and w_i is the weight for track i,

$$w_i = \frac{\sin^2\theta_i}{\sigma_{T_i}} \tag{10}$$

where θ_i is the angle between track i and the vertex axis and σ_{T_i} is an estimate of the uncertainty of the impact parameter of track i to the vertex axis calculated from the appropriate components of the track resolution σ_{xy} and σ_z. The above selection criteria yield a sample of 3291 decays. Monte Carlo simulation shows that there is an enhancement by a factor of 2.5 of B^0_d with respect to B^+_u decays in this sample due to the vertex charge = 0 requirement. Fig. 4 shows the charge dipole distribution for data compared with the Monte Carlo. Also shown are the MC distributions for $B^0_d(\bar{b})$ and $\overline{B^0_d}(b)$ separately.

The analyzing power for this final state tag increases with the magnitude of δq, reaching a maximum of 68% in the tails. The purity of b quarks in vertices selected in Monte Carlo is used to parametrize the probability of a successful dipole tag as

$$P_D = 0.84\, e^{-|2.4\times|\delta q|-0.8|^3} \tag{11}$$

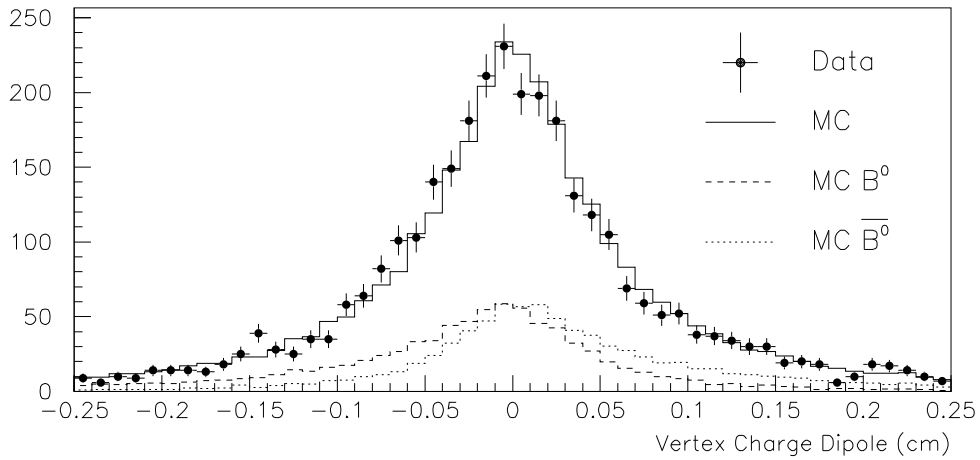

Figure 4: Distribution of the reconstructed charge dipole δq.

where $P_D(b) = P_D$ or $1 - P_D$ for $\delta q > 0$ or $\delta q < 0$ respectively. The final charge dipole selection cut requires $\delta q < 0.5$ cm. The dipole can be used to tag the final state b quark for B_s^0 and B_u^+ decays is well as for B_d^0 mesons. The charge dipole is not sensitive to the total vertex charge since it is defined in terms of the spatial displacement between a center of positive and center of negative charge. The analyzing power is greatest for B_s^0 decays since a higher fraction of the cascade charm decays carry charge through the dominant $B_s^0 \to D_s^- X$ mode. For B_u^+ the analyzing power of δq is found from Monte Carlo studies to be similar to B_d^0 and the B_u^+ mesons are used as a demonstration of the charge dipole. An independent sample of topological vertices is selected using the same vertex requirements as above, except with total track charge equal to ± 1 rather than 0. Vertices of total charge equal to $+1$ (-1) are $\sim 50\%$ pure in B_u^+ (B_u^-) meson decays for which a negative (positive) charge dipole is expected due to the cascade decay charge structure. Fig 5 shows that the δq distribution for both cases has the predicted asymmetry and that the data agrees with the Monte Carlo simulation.

A further cross-check is made from the same sample using the polarized forward-backward asymmetry of b quark production, used for an initial state tag, to verify the charge dipole as follows. The polar angle θ_T of the event thrust axis, directed toward the vertex hemisphere, is determined. Distributions of $\cos\theta_T$ signed by the product of e^- beam polarization and reconstructed charge dipole for these vertices is shown in Fig. 6 (separately for 1993 and 1994-95 with average beam polarizations of 63% and 77% respectively). As well as being rich in $B_u^\pm$ meson decays, for B_d^0 decays surviving the ± 1 charge cut δq is not well measured since the charge reconstruction is incorrect. It can be seen that the B_d^0 decays contribute little to the observed asymmetry in Fig. 6 in part due to their relatively poor charge reconstruction and in part due to $B_d^0 - \overline{B_d^0}$ mixing. The observed asymmetry is the result of the forward-backward production asymmetry of the b quark constituent of the B_u^+ mesons where the same decaying b quark has been tagged using the vertex charge dipole. Each entry in Fig. 6 is weighted by its analyzing power, which is a function of $\mid \delta q \mid$ and

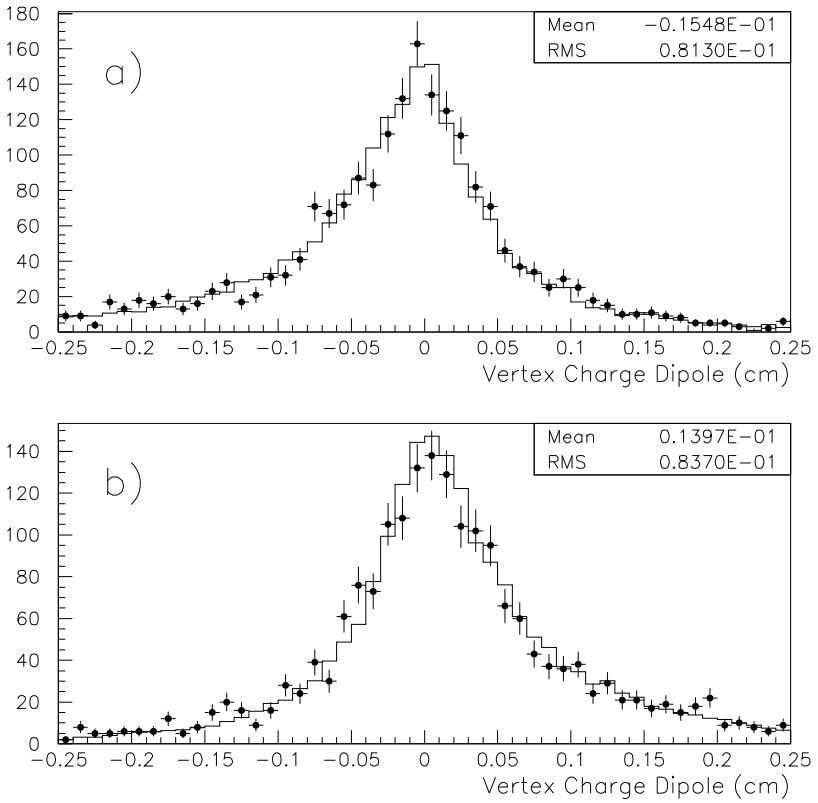

Figure 5: Reconstructed charge dipole for vertices with total charge of a) $+1$ and b) -1 for data (points) and MC (solid line).

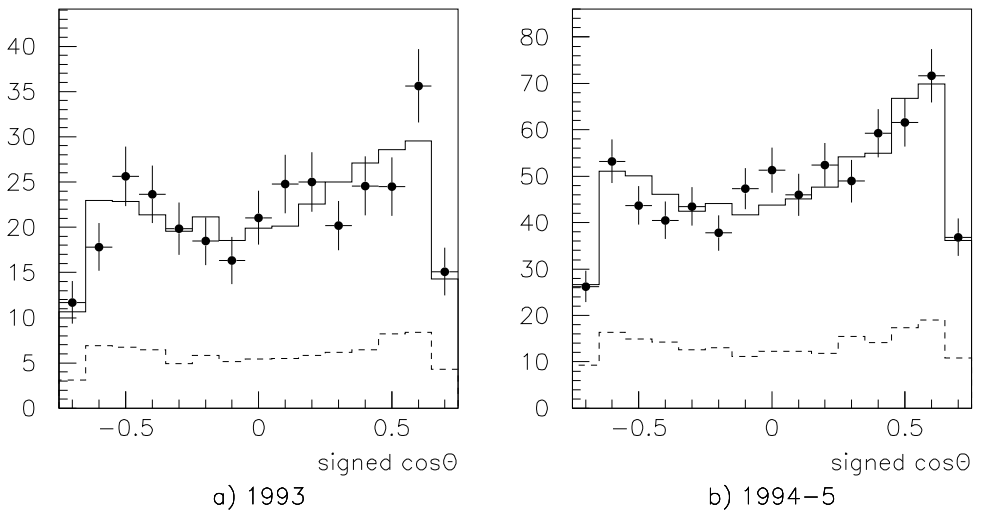

Figure 6: Polarization asymmetry with charge dipole for data (points) and full MC (solid line) with MC B_d^0 contribution (dashed line).

the error bars shown on the data points are calculated accordingly.

The distributions in Fig. 6 are only weakly dependent upon the MC value of Δm_d. This latter quantity is measured in the data by using the sample of vertices of charge zero, i.e. with the correct charge reconstruction for B_d^0 and an enhanced neutral B meson purity. The tagged mixed fraction of B_d^0 candidates is obtained as a function of decay length in order to observe the time dependent mixing. The measurement is enhanced by combining the polarization with jet charge to improve the initial b state tag purity.

4 Oscillation Frequency Measurement

The initial state tag probability $P_i(b)$ (Eq. 8) and the probability of the final state tag $P_f(b)$ (kaon $P_K(b)$ or dipole $P_D(b)$ Eq. 11) each have an analyzing power $a_{i,f} = |2P_{i,f} - 1|$. The probability that a B_d^0 candidate changed state or 'mixed', that is an initial state b ($\overline{b}$) quark leading to a final state $\overline{b}$ (b) quark, is

$$P_M = P_i(b)P_f(\overline{b}) + P_i(\overline{b})P_f(b) \ , \tag{12}$$

with overall tag analyzing power $a_t = |2P_M - 1|$ (or simply $a_i a_f$). The B_d^0 time dependent mixing parameter is extracted using a χ^2 fit of the data mixed fraction to the Monte Carlo in bins of reconstructed decay length. The mixed fraction in each bin is the number of vertices tagged as mixed ($P_M > 0.5$) divided by the total with each vertex weighted by a_t to optimize the tag information.

The χ^2 fit is made to the MC for a range of Δm_d values by generating MC mixed fraction distributions for arbitrary Δm_d in the following way. The MC B_d^0 mixing is 'switched off' by reversing the sign of the final state tag if the decay vertex is a Monte Carlo $B_d^0(\overline{B_d^0})$ which was initially produced as a $\overline{B_d^0}(B_d^0)$. Using this $\Delta m_d = 0$ Monte Carlo, two decay length distributions are generated labelled M_0 and U_0 for vertices tagged as mixed ($P_M > 0.5$) and unmixed ($P_M < 0.5$) respectively with entries weighted by a_t. Corresponding distributions for arbitrary Δm_d, labelled $M_{\Delta m_d}$ and $U_{\Delta m_d}$, are then generated by combining the entries M_0^i and U_0^i in M_0 and U_0 respectively using a further weight W^i:

$$W^i = \frac{1}{2}\left(1 + \cos \Delta m_d \, t^i\right) \ , \tag{13}$$

which is the probability that a b quark remains a b quark given the mixing parameter Δm_d and a B_d^0 meson i decaying after the MC proper time t^i. The weight is calculated and applied to each entry in the original histograms as indicated below

$$M_{\Delta m_d} = \sum W^i M_0^i + \sum (1 - W^i) U_0^i \ ,$$

$$U_{\Delta m_d} = \sum W^i U_0^i + \sum (1 - W^i) M_0^i \ ,$$

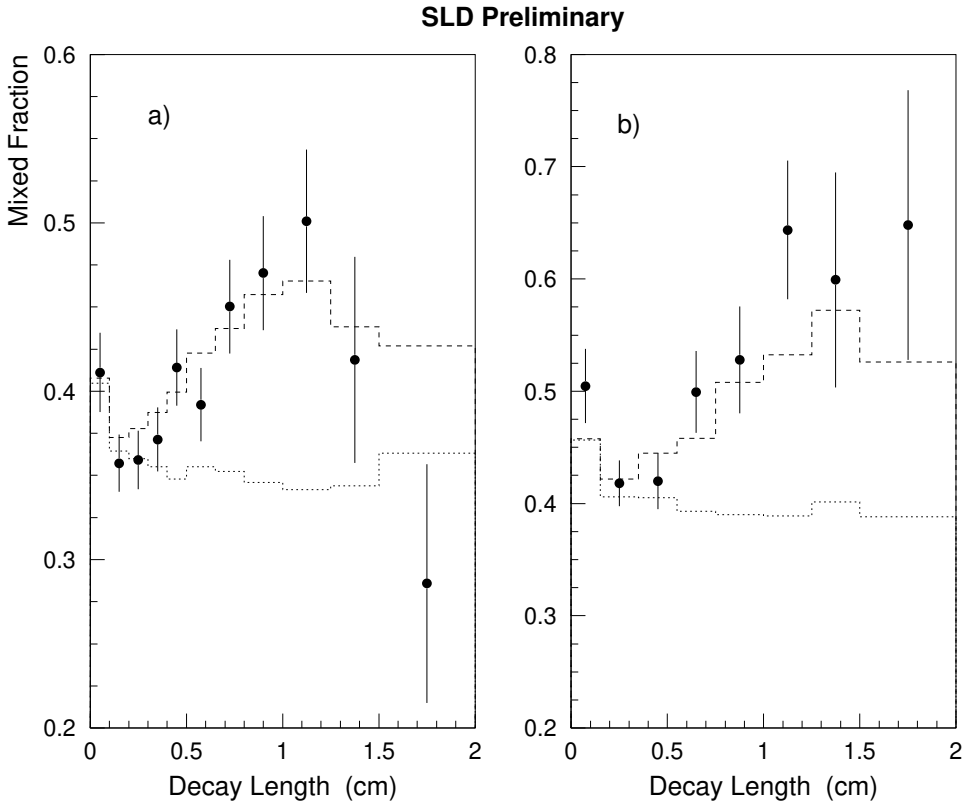

Figure 7: Fraction of mixed decays as a function of decay length for the kaon tag (a) and dipole charge tag (b) analyses. Shown are data (points), best fit MC (dashed histograms) and MC without B_d^0 mixing (dotted histograms).

where the sum is applied to each bin in decay length. The MC mixed fraction $\frac{M_{\Delta m_d}}{M_{\Delta m_d}+U_{\Delta m_d}}$ follows trivially and the χ^2 of the data fit to the MC is determined as a function of Δm_d in order to derive the B_d^0 mixing parameter in the data. The fit procedure is cross checked by dividing the MC into 12 equal samples (each about the same size as the real data) and fitting each sample in turn as 'data' to the remaining MC. The mean result of the 12 fits agrees with the MC input value of Δm_d for both final state tags, and the RMS spread of the 12 fits is consistent with the statistical error of the fit.

The results of the fits to the data are shown in Fig. 7. The fits yield measurements of $\Delta m_d = 0.580 \pm 0.066$ ps^{-1} with a χ^2/dof of 10.2/10 for the kaon tag and $\Delta m_d = 0.561 \pm 0.078$ ps^{-1} with a χ^2/dof of 8.8/7 for the charge dipole tag.

5 Systematic Uncertainties

The total systematic error extracted below includes effects due to the uncertainty in the detector and physics modeling, and in the fitting technique. The results are summarized in Table 1. In this section, systematic uncertainties common to both kaon and charge dipole analyses are described first, followed by uncertainties specific to each analysis.

The systematic contribution due to uncertainties in detector modeling include tracking efficiency, detector resolution, and kaon identification efficiency. A discrepancy in the average number of tracks was observed comparing data and Monte Carlo simulation. This was corrected for in the simulation by removing the appropriate number of tracks, taking into account the effect of the dependence on track p_T, $\cos\theta$, azimuthal angle and angle between the track and the nearest jet axis. On average, 3.8% of the tracks used in this analysis were removed from the simulation. We assigned as a systematic uncertainty the entire difference between fit results obtained with and without this track efficiency correction. Detailed checks of the track resolution modeling were also performed. It was found that the simulation reproduces the distribution of the track impact parameter in the $r\phi$ plane very well, but appeared to be somewhat narrower than the data in the core of the impact parameter distribution in the rz plane. This is attributed to residual misalignments within the VXD. A correction was applied to account for this and the quoted systematic uncertainty corresponds to the difference between results obtained with and without this correction.

We have studied the sensitivity of the measurement to the production characteristics of B hadrons in Z^0 decays, as well as to the B and D decay models. In this analysis, the fraction of B_u^+ and B_d^0 produced in $Z^0 \to b\,\bar{b}$ are assumed to be equal. However, we varied the fraction of B_s^0 and B baryons by 0.115 ± 0.030 and 0.072 ± 0.040 respectively. The uncertainty in the fragmentation of the b-quark was studied by varying the value of ϵ in the Peterson *et al.* fragmentation parametrization, such as to modify the mean fractional energy of B hadrons according to $\langle x_E \rangle = 0.700 \pm 0.011$ [11]. The dependence on the shape of the $\langle x_E \rangle$ distribution was also included in the total fragmentation uncertainty [12].

The sensitivity to the B decay model was investigated by varying branching ratios, track multiplicities and lifetimes. The average B decay multiplicity was varied by ± 0.3 tracks [13]. Differences in lifetime between different B hadron types would affect the shape of the distribution of the mixed fraction of decays. Therefore, the lifetime of each B hadron type was varied separately following $\tau(B_u) = 1.55 \pm 0.10$ ps, $\tau(B_d) = 1.55 \pm 0.10$ ps, $\tau(B_s) = 1.55 \pm 0.15$ ps, and $\tau(B_{baryon}) = 1.10 \pm 0.11$ ps. The mixing parameter Δm_s for B_s^0 mixing was set to 6.45 in the simulation. Sensitivity to this parameter was examined by varying Δm_s from 5 to ∞. Charm hadron lifetimes were varied according to the uncertainty in the world average values [8].

Systematic error	Uncertainty in Δm_d (ps^{-1})	
	Kaon Tag	Dipole Charge Tag
	Detector Modeling	
Tracking efficiency	0.006	0.010
Detector resolution	0.003	0.003
Kaon ID efficiency	0.035	—
	Physics Modeling	
B_s fraction	0.016	0.007
B baryon fraction	0.021	0.003
b fragmentation	0.015	0.011
K^-, K^+ production	0.030	—
B.R.($B \to D^0 X, D^+ X$)	—	0.010
B.R.($B \to D\ D\ X$)	—	0.006
B multiplicity	0.005	0.008
B_u lifetime	0.010	0.001
B_d lifetime	0.004	0.008
B_s lifetime	0.010	0.002
B baryon lifetime	0.002	0.001
B_s mixing	0.005	0.009
Charm decay multiplicity	—	0.002
Charm decay K^0 production	—	0.009
Charm lifetime	0.008	0.003
Initial state tag	0.010	0.010
	Monte Carlo and Fitting	
Fit Systematics	0.042	0.016
MC Statistics	0.017	0.021
Total	0.075	0.039

Table 1: Summary of contributions to the systematic uncertainty in Δm_d for the kaon tag and charge dipole tag analyses.

The parameters relevant to the parametrizations of the initial state tag were varied as follows: $A_b = 0.94 \pm 0.04$, $\Delta P_e = \pm 1\%$, and $\Delta\alpha = \pm 0.02$. The fit systematics were determined by taking the RMS of the changes in the fit value using a variety of decay length ranges and binning.

For the kaon tag analysis, an additional uncertainty arises from the modeling of the kaon identification performance. The $\pi \to K$ misidentification in the simulation was calibrated using a pure sample of pions from $K^0_s \to \pi^+\pi^-$ decays in hadronic Z^0 events from the data. The corresponding systematic uncertainty was taken to be half of the difference between Δm_d values obtained with and without this calibration correction. Furthermore, the analyzing power of the kaon tag relies on the accurate modeling of right-sign and wrong-sign kaon production. To account for uncertainties

in this modeling, the mean number of right-sign and wrong-sign kaons from B_u^+ and B_d^0 decays was varied by ± 0.1 while keeping the average number of kaons unchanged (i.e. the means for right-sign and wrong-sign kaons were varied in an anticorrelated way). This range is slightly more conservative than the uncertainty in the ARGUS measurement [10].

The charge dipole relies on the topological separation between the B and D decay products, and therefore is potentially sensitive to the modeling of D^+ and D^0 production and decay due to the large lifetime difference between these two mesons. To investigate this, the branching ratios for $B_u^+ \to D^- X$, $B_u^+ \to \overline{D^0} X$, $B_d^0 \to D^- X$, and $B_d^0 \to \overline{D^0} X$ were varied according to 0.173 ± 0.074, 0.632 ± 0.052, 0.261 ± 0.074, and 0.546 ± 0.052 respectively. These uncertainties correspond to twice the uncertainties in the inclusive measurements performed at the $\Upsilon(4s)$ [6] as there is no information regarding the separate branching ratios for B_u^+ and B_d^0. The fraction of decays of the type $B \to DDX$ was taken to be 0.15 ± 0.05. The sensitivity to the D decay model was investigated by modifying the D decay multiplicities and K^0 production rates according to existing measurements [14].

6 Summary

From 150,000 Z^0 decays collected by SLD between 1993 and 1995 two measurements of the $B_d^0 - \overline{B_d^0}$ mixing parameter Δm_d have been performed using a novel topological vertexing technique. Initial state tagging is provided by the SLC e^- beam polarization together with a jet charge technique. Final state tagging used the charge of identified kaons attached to the secondary vertex or the charge dipole of all the tracks in the vertex. The preliminary results obtained for the final state kaon tag and the vertex charge dipole are, respectively:

$$\Delta m_d = 0.58 \pm 0.07(\text{stat}) \pm 0.08(\text{syst})\ \text{ps}^{-1}\ , \tag{14}$$

$$\Delta m_d = 0.56 \pm 0.08(\text{stat}) \pm 0.04(\text{syst})\ \text{ps}^{-1}\ . \tag{15}$$

We thank the personnel of the SLAC accelerator department and the technical staffs of our collaborating institutions for their outstanding efforts.

References

[1] K. Abe *et al.*, Phys. Rev. **D53**, 1023 (1996).

[2] T. Sjöstrand, CERN-TH-7112-93, Feb. 1994.

[3] R. Brun *et al.*, CERN-DD/EE/84-1, 1989.

[4] C. Peterson *et al.*, Phys. Rev. **D27**, 105 (1983).

[5] CLEO QQ MC code provided by P. Kim and the CLEO Collaboration.

[6] CLEO Collaboration: B. Barish *et al.*, **CLNS-95-1362** (1995);
ARGUS Collaboration: H. Albrecht *et al.*, *Z. Phys.* **C58**, 191 (1993);
ARGUS Collaboration: H. Albrecht *et al.*, *Z. Phys.* **C62**, 371 (1994);
F. Muheim (CLEO Collaboration), talk presented at the 8th DPF Meeting, Albuquerque, New Mexico, Aug 1994;
M. Thulasidas, Ph.D thesis, Syracuse University (1993);
CLEO Collaboration: G. Crawford *et al.*, *Phys. Rev.* **D45**, 752 (1992)
CLEO Collaboration: D. Bortoletto *et al.*, *Phys. Rev.* **D45**, 21 (1992).

[7] T.R. Junk, Ph.D. Thesis, Stanford University, SLAC-Report-95-476, Nov. 1995.

[8] Particle Data Group, Phys. Rev. **D50**, Part I (1994).

[9] D. J. Jackson, *A Topological Vertex Reconstruction Algorithm for Hadronic Jets*, submitted to *Nucl. Inst. and Meth.*, SLAC-PUB-7215, July 1996.

[10] H.Albrecht *et al.*, Z. Phys. **C62**, 371 (1994).

[11] see for example,
R. Akers *et al.*, Z. Phys. **C60**, 199 (1993);
D. Buskulic *et al.*, Z. Phys. **C62**, 179 (1994);
P. Abreu *et al.*, Z. Phys. **C66**, 323 (1995).

[12] M. G. Bowler, Z. Phys. **C11**, 169 (1981).

[13] H.Albrecht *et al.*, Z. Phys. **C54**, 13 (1992);
R.Giles *et al.*, Phys. Rev. **D30**, 2279 (1984).

[14] D.Coffman *et al.*, Phys. Lett. **B263**, 135 (1991);

*List of Authors

K. Abe,[19] K. Abe,[29] I. Abt,[13] T. Akagi,[27] N.J. Allen,[4] W.W. Ash,[27]†
D. Aston,[27] K.G. Baird,[24] C. Baltay,[33] H.R. Band,[32] M.B. Barakat,[33]
G. Baranko,[9] O. Bardon,[15] T. Barklow,[27] A.O. Bazarko,[10] R. Ben-David,[33]
A.C. Benvenuti,[2] G.M. Bilei,[22] D. Bisello,[21] G. Blaylock,[6] J.R. Bogart,[27]
B. Bolen,[17] T. Bolton,[10] G.R. Bower,[27] J.E. Brau,[20] M. Breidenbach,[27]
W.M. Bugg,[28] D. Burke,[27] T.H. Burnett,[31] P.N. Burrows,[15] W. Busza,[15]
A. Calcaterra,[12] D.O. Caldwell,[5] D. Calloway,[27] B. Camanzi,[11]
M. Carpinelli,[23] R. Cassell,[27] R. Castaldi,[23][a] A. Castro,[21]
M. Cavalli-Sforza,[6] A. Chou,[27] E. Church,[31] H.O. Cohn,[28] J.A. Coller,[3]
V. Cook,[31] R. Cotton,[4] R.F. Cowan,[15] D.G. Coyne,[6] G. Crawford,[27]

A. D'Oliveira,[7] C.J.S. Damerell,[25] M. Daoudi,[27] R. De Sangro,[12]
R. Dell'Orso,[23] P.J. Dervan,[4] M. Dima,[8] D.N. Dong,[15] P.Y.C. Du,[28]
R. Dubois,[27] B.I. Eisenstein,[13] R. Elia,[27] E. Etzion,[4] D. Falciai,[22] C. Fan,[9]
M.J. Fero,[15] R. Frey,[20] K. Furuno,[20] T. Gillman,[25] G. Gladding,[13]
S. Gonzalez,[15] G.D. Hallewell,[27] E.L. Hart,[28] J.L. Harton,[8] A. Hasan,[4]
Y. Hasegawa,[29] K. Hasuko,[29] S. J. Hedges,[3] S.S. Hertzbach,[16]
M.D. Hildreth,[27] J. Huber,[20] M.E. Huffer,[27] E.W. Hughes,[27] H. Hwang,[20]
Y. Iwasaki,[29] D.J. Jackson,[25] P. Jacques,[24] J. A. Jaros,[27] A.S. Johnson,[3]
J.R. Johnson,[32] R.A. Johnson,[7] T. Junk,[27] R. Kajikawa,[19] M. Kalelkar,[24]
H. J. Kang,[26] I. Karliner,[13] H. Kawahara,[27] H.W. Kendall,[15] Y. D. Kim,[26]
M.E. King,[27] R. King,[27] R.R. Kofler,[16] N.M. Krishna,[9] R.S. Kroeger,[17]
J.F. Labs,[27] M. Langston,[20] A. Lath,[15] J.A. Lauber,[9] D.W.G.S. Leith,[27]
V. Lia,[15] M.X. Liu,[33] X. Liu,[6] M. Loreti,[21] A. Lu,[5] H.L. Lynch,[27] J. Ma,[31]
G. Mancinelli,[22] S. Manly,[33] G. Mantovani,[22] T.W. Markiewicz,[27]
T. Maruyama,[27] H. Masuda,[27] E. Mazzucato,[11] A.K. McKemey,[4]
B.T. Meadows,[7] R. Messner,[27] P.M. Mockett,[31] K.C. Moffeit,[27]
T.B. Moore,[33] D. Muller,[27] T. Nagamine,[27] S. Narita,[29] U. Nauenberg,[9]
H. Neal,[27] M. Nussbaum,[7] Y. Ohnishi,[19] L.S. Osborne,[15] R.S. Panvini,[30]
H. Park,[20] T.J. Pavel,[27] I. Peruzzi,[12][b] M. Piccolo,[12] L. Piemontese,[11]
E. Pieroni,[23] K.T. Pitts,[20] R.J. Plano,[24] R. Prepost,[32] C.Y. Prescott,[27]
G.D. Punkar,[27] J. Quigley,[15] B.N. Ratcliff,[27] T.W. Reeves,[30] J. Reidy,[17]
P.E. Rensing,[27] L.S. Rochester,[27] P.C. Rowson,[10] J.J. Russell,[27]
O.H. Saxton,[27] T. Schalk,[6] R.H. Schindler,[27] B.A. Schumm,[14] S. Sen,[33]
V.V. Serbo,[32] M.H. Shaevitz,[10] J.T. Shank,[3] G. Shapiro,[14] D.J. Sherden,[27]
K.D. Shmakov,[28] C. Simopoulos,[27] N.B. Sinev,[20] S.R. Smith,[27] M.B. Smy,[8]
J.A. Snyder,[33] P. Stamer,[24] H. Steiner,[14] R. Steiner,[1] M.G. Strauss,[16]
D. Su,[27] F. Suekane,[29] A. Sugiyama,[19] S. Suzuki,[19] M. Swartz,[27]
A. Szumilo,[31] T. Takahashi,[27] F.E. Taylor,[15] E. Torrence,[15] A.I. Trandafir,[16]
J.D. Turk,[33] T. Usher,[27] J. Va'vra,[27] C. Vannini,[23] E. Vella,[27]
J.P. Venuti,[30] R. Verdier,[15] P.G. Verdini,[23] S.R. Wagner,[27] A.P. Waite,[27]
S.J. Watts,[4] A.W. Weidemann,[28] E.R. Weiss,[31] J.S. Whitaker,[3]
S.L. White,[28] F.J. Wickens,[25] D.A. Williams,[6] D.C. Williams,[15]
S.H. Williams,[27] S. Willocq,[33] R.J. Wilson,[8] W.J. Wisniewski,[27]
M. Woods,[27] G.B. Word,[24] J. Wyss,[21] R.K. Yamamoto,[15] J.M. Yamartino,[15]
X. Yang,[20] S.J. Yellin,[5] C.C. Young,[27] H. Yuta,[29] G. Zapalac,[32]
R.W. Zdarko,[27] C. Zeitlin,[20] and J. Zhou,[20]

[1] *Adelphi University, Garden City, New York 11530*
[2] *INFN Sezione di Bologna, I-40126 Bologna, Italy*
[3] *Boston University, Boston, Massachusetts 02215*
[4] *Brunel University, Uxbridge, Middlesex UB8 3PH, United Kingdom*
[5] *University of California at Santa Barbara, Santa Barbara, California 93106*
[6] *University of California at Santa Cruz, Santa Cruz, California 95064*

[7] *University of Cincinnati, Cincinnati, Ohio 45221*
[8] *Colorado State University, Fort Collins, Colorado 80523*
[9] *University of Colorado, Boulder, Colorado 80309*
[10] *Columbia University, New York, New York 10027*
[11] *INFN Sezione di Ferrara and Università di Ferrara, I-44100 Ferrara, Italy*
[12] *INFN Lab. Nazionali di Frascati, I-00044 Frascati, Italy*
[13] *University of Illinois, Urbana, Illinois 61801*
[14] *Lawrence Berkeley Laboratory, University of California, Berkeley, California 94720*
[15] *Massachusetts Institute of Technology, Cambridge, Massachusetts 02139*
[16] *University of Massachusetts, Amherst, Massachusetts 01003*
[17] *University of Mississippi, University, Mississippi 38677*
[19] *Nagoya University, Chikusa-ku, Nagoya 464 Japan*
[20] *University of Oregon, Eugene, Oregon 97403*
[21] *INFN Sezione di Padova and Università di Padova, I-35100 Padova, Italy*
[22] *INFN Sezione di Perugia and Università di Perugia, I-06100 Perugia, Italy*
[23] *INFN Sezione di Pisa and Università di Pisa, I-56100 Pisa, Italy*
[24] *Rutgers University, Piscataway, New Jersey 08855*
[25] *Rutherford Appleton Laboratory, Chilton, Didcot, Oxon OX11 0QX United Kingdom*
[26] *Sogang University, Seoul, Korea*
[27] *Stanford Linear Accelerator Center, Stanford University, Stanford, California 94309*
[28] *University of Tennessee, Knoxville, Tennessee 37996*
[29] *Tohoku University, Sendai 980 Japan*
[30] *Vanderbilt University, Nashville, Tennessee 37235*
[31] *University of Washington, Seattle, Washington 98195*
[32] *University of Wisconsin, Madison, Wisconsin 53706*
[33] *Yale University, New Haven, Connecticut 06511*
† *Deceased*
[a] *Also at the Università di Genova*
[b] *Also at the Università di Perugia*